

Supporting Information

## **Graphene Oxide Coupled Carbon Nitride Homo-Heterojunction Photocatalyst for Enhanced Hydrogen Production**

Mohammad Rahman<sup>a</sup>, Jun Zhang<sup>b</sup>, Youhong Tang<sup>c</sup>, Kenneth Davey<sup>a</sup> and Shi-Zhang Qiao<sup>a\*</sup>

\*E-mail: s.qiao@adelaide.edu.au

<sup>a</sup>School of Chemical Engineering, The University of Adelaide, Adelaide, SA 5005, Australia

<sup>b</sup>State Key Laboratory of Advanced Technology for Materials Synthesis and Processing,  
Wuhan University of Technology, Wuhan 430070, PR China

<sup>c</sup>School of Computer Science, Engineering and Mathematics, Flinders University, Adelaide,  
SA 5001, Australia

## I. Experimental Section

### 1. Synthesis of GO

Graphene oxide (GO) was synthesized from graphite by following the modified Hummers' method.<sup>1,2</sup> In a typical synthesis, graphitic flakes (5 g), condensed H<sub>2</sub>SO<sub>4</sub> (15 mL, 98%), K<sub>2</sub>S<sub>2</sub>O<sub>8</sub> (2.5 g), and P<sub>2</sub>O<sub>5</sub> (2.5 g) were added together at 80 °C and kept for 6 h. When the mixture reached room temperature (RT), DI water was used to wash the product until pH = 7. The product was then filtered and dried at 60 °C. Pre-oxidized graphite and KMnO<sub>4</sub> (15 g) were added sequentially and slowly into a beaker with 115 mL of condensed H<sub>2</sub>SO<sub>4</sub> in an ice-bath under stirring; the temperature was maintained below 20 °C. The resultant product was kept at 35 °C for 3.5 h and 98 °C for 15 min, respectively. Then DI water and 6.5 mL of H<sub>2</sub>O<sub>2</sub> (30%) were added, and the solution turned to brilliant yellow. Finally, the product was again washed with DI water and 115 mL of HCL (1/10, v/v). The dialysis continued for several days and GO solution (0.5 mg mL<sup>-1</sup>) was obtained by ultra-sonication for 30 min in a probe sonicator (950 W, 30% amplitude) and centrifugation at 3000 rpm for 30 min.

## II. Supplementary Results

**Table S1** A summary of recently reported ternary photocatalysts. In all cases for hydrogen production, Pt was used as a co-catalyst.

Ternary hybrid	Application	HER	Ref.
GCN/ACN/GO	H <sub>2</sub> production	251 $\mu\text{mol h}^{-1}$	This work
NiS/Zn <sub>x</sub> Cd <sub>1-x</sub> S/rGO	H <sub>2</sub> production	375.7 $\mu\text{mol h}^{-1}$	3
GCN/N-GR/MoS <sub>2</sub> /	Degradation of MB	-	4
GCN/CdS/rGO	Degradation of RhB	-	5
CeO <sub>2</sub> /GCN/rGO	Degradation of RhB	-	6
GCN/ZnO/Fe <sub>2</sub> O <sub>3</sub>	Water treatment	-	7
Ag/AgCl/GCN	Degradation of MO	-	8
Pt/SnO <sub>x</sub> /TiO <sub>2</sub>	H <sub>2</sub> production	4.04 $\text{mmol h}^{-1}\text{g}^{-1}$	9
CdS/ TiO <sub>2</sub> /Pt	H <sub>2</sub> production	6 – 9 $\text{mmol h}^{-1}\text{g}^{-1}$	10
ZnO/Pt/CdS	H <sub>2</sub> production	17.4 $\text{mmol h}^{-1}\text{g}^{-1}$	11
ZnO/Pt/Cd <sub>1-x</sub> Zn <sub>x</sub> S	H <sub>2</sub> production	36.5 $\text{mmol h}^{-1}\text{g}^{-1}$	11
ZnO/Pt/CdS <sub>1-x</sub> Se <sub>x</sub>	H <sub>2</sub> production	-	11
Ni(OH) <sub>2</sub> /CdS/rGO	H <sub>2</sub> production	4.73 $\text{mmol h}^{-1}\text{g}^{-1}$	12
Ag <sub>2</sub> CO <sub>3</sub> /Ag/AgCl	Degradation of MB	-	13
graphene/g-C <sub>3</sub> N <sub>4</sub> /α-S <sub>8</sub>	Bacterial inactivation	-	14
N-graphene/ g-C <sub>3</sub> N <sub>4</sub> / MoS <sub>2</sub>	Li-ion batteries	-	15
MoS <sub>2</sub> /GO/ g-C <sub>3</sub> N <sub>4</sub>	Degradation of RhB	-	16

**Table S2** Comparison of deconvoluted XPS C1s spectra. Binding energies (BE) and concentration (%) of C1s core electrons of two kinds of carbon species recorded for GCN, ACN and GCN/ACN/GO (see Fig. S7 a-c).

Sample	C1		C2	
	<i>B.E. (eV)</i>	<i>% conc.</i>	<i>B.E. (eV)</i>	<i>% conc.</i>
GCN	288.15	53.15	284.58	46.65
ACN	287.88	68.57	284.58	31.43
GCN/ACN/GO	287.66	59.33	284.6	40.67

**Table S3** Comparison of deconvoluted XPS N1s spectra. Binding energies (BE) and concentration (%) of N1s core electrons of three kinds of nitrogen species recorded for GCN, ACN and GCN/ACN/GO (see Fig. S7 d-f).

Sample	N1		N2		N3	
	<i>B.E. (eV)</i>	<i>% conc.</i>	<i>B.E. (eV)</i>	<i>% conc.</i>	<i>B.E. (eV)</i>	<i>% conc.</i>
GCN	398.32	76.75	399.89	21.48	396.43	1.77
ACN	398.21	71.6	400	27.31	396.32	1.62
GCN/ACN/GO	397.87	65.82	399.61	28.21	395.85	5.97

“Tauc plot” has been adopted to calculate the bandgap of ACN and GCN (Fig. S15). Mott-Schottky plot has been used to determine the conduction band (CB) position (Fig. S16). The calculated data are summarized in Table S4.

**Table S4** Calculated band positions and band gap.

Photocatalysts	$E_{CB}$ (V vs. NHE)	$E_{VB}$ (V vs. NHE)	$E_g$ (eV)
ACN	-0.91	1.64	2.55
GCN	-1.5	1.1	2.6

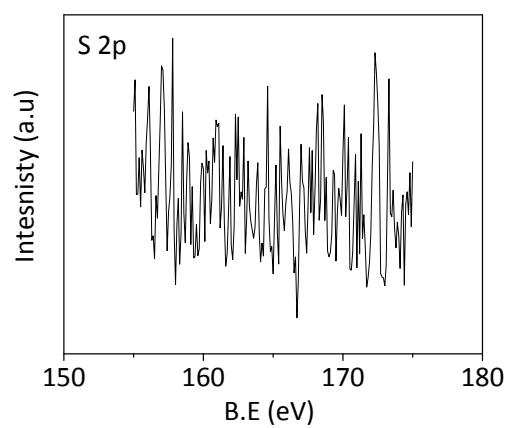


**Fig. S1** XPS spectra of S 2P.

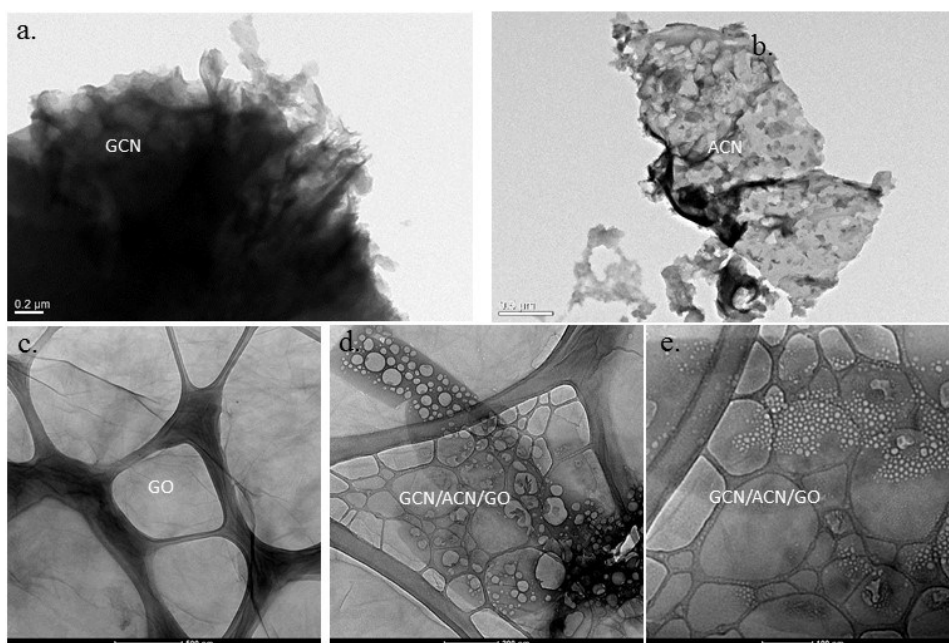


**Fig. S2** TEM images of (a) GCN, (b) ACN, (c) GO and (d-e) GCN/ACN/GO.

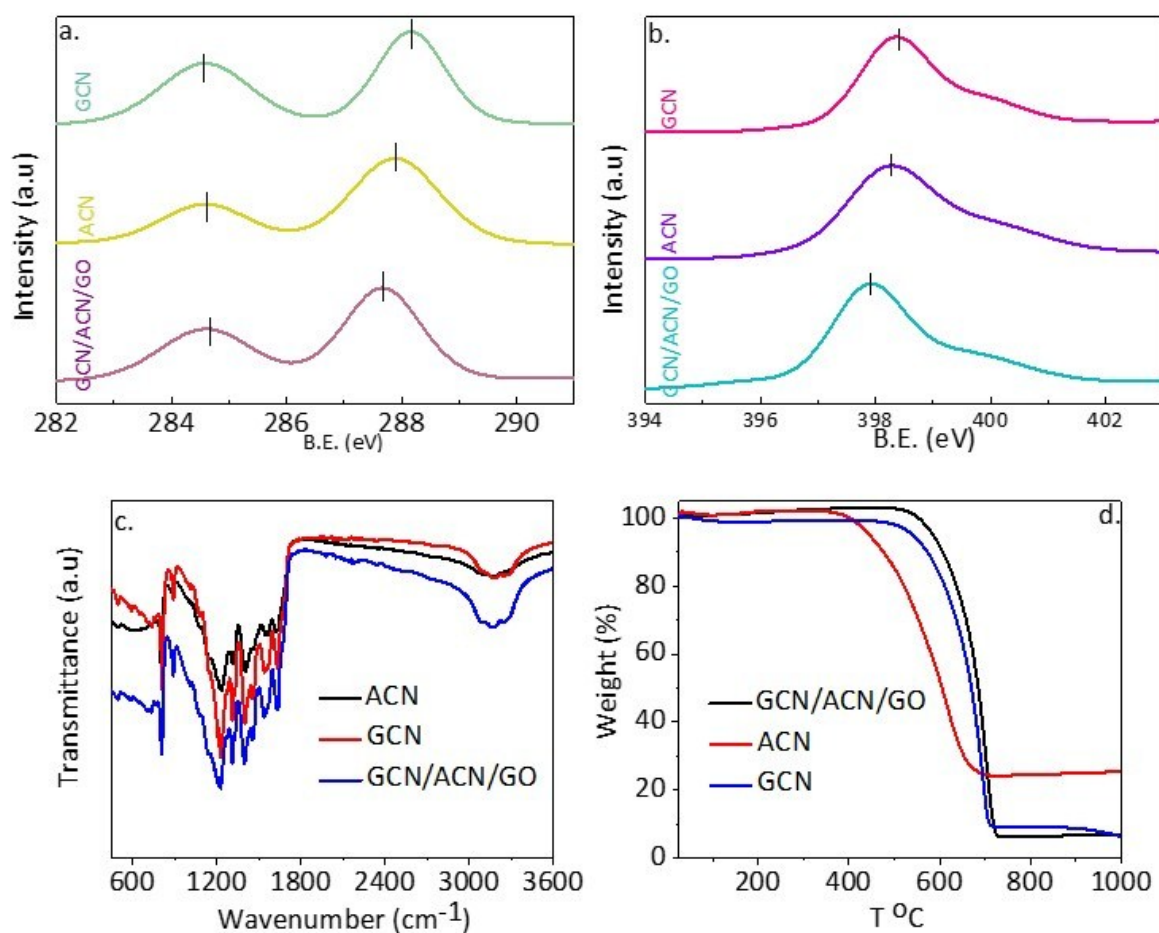


**Fig. S3** (a) Envelope of XPS C1s spectra, (b) Envelope of XPS N1s spectra (c) FTIR spectra and (d) TGA spectra of GCN, ACN and GCN/ACN/GO.

Fig S3(a-b) is showing the envelope of XPS C1s and N1s spectra, respectively for GCN, ACN and GCN/ACN/GO. The position of peaks that resemble C=C-C bonding at around 284.5 eV is relatively unchanged, whereas the position of peaks for N=C-N is left shifted. It indicates that there is a change in valence between C and N upon integration of GCN and ACN in ternary hybrid. This is also supported by a corresponding left shift for the peak positions of C=N-C bonds in N1s spectra. The C-N heterocycles in FTIR spectra of ACN is highly diffused where it is highly pronounced in GCN and ternary hybrid. This implies that a hybridization is occurred between GCN and ACN to form the ternary structure. Upon hybridization, the stability of ternary hybrid should be higher than that of individual ACN and GCN. This is clearly evident in the corresponding TGA profile. From these combined studies of XPS, FTIR and TGA, we can confidently conclude that ACN and GCN is hybridized to form GCN/ACN/GO ternary hybrid.

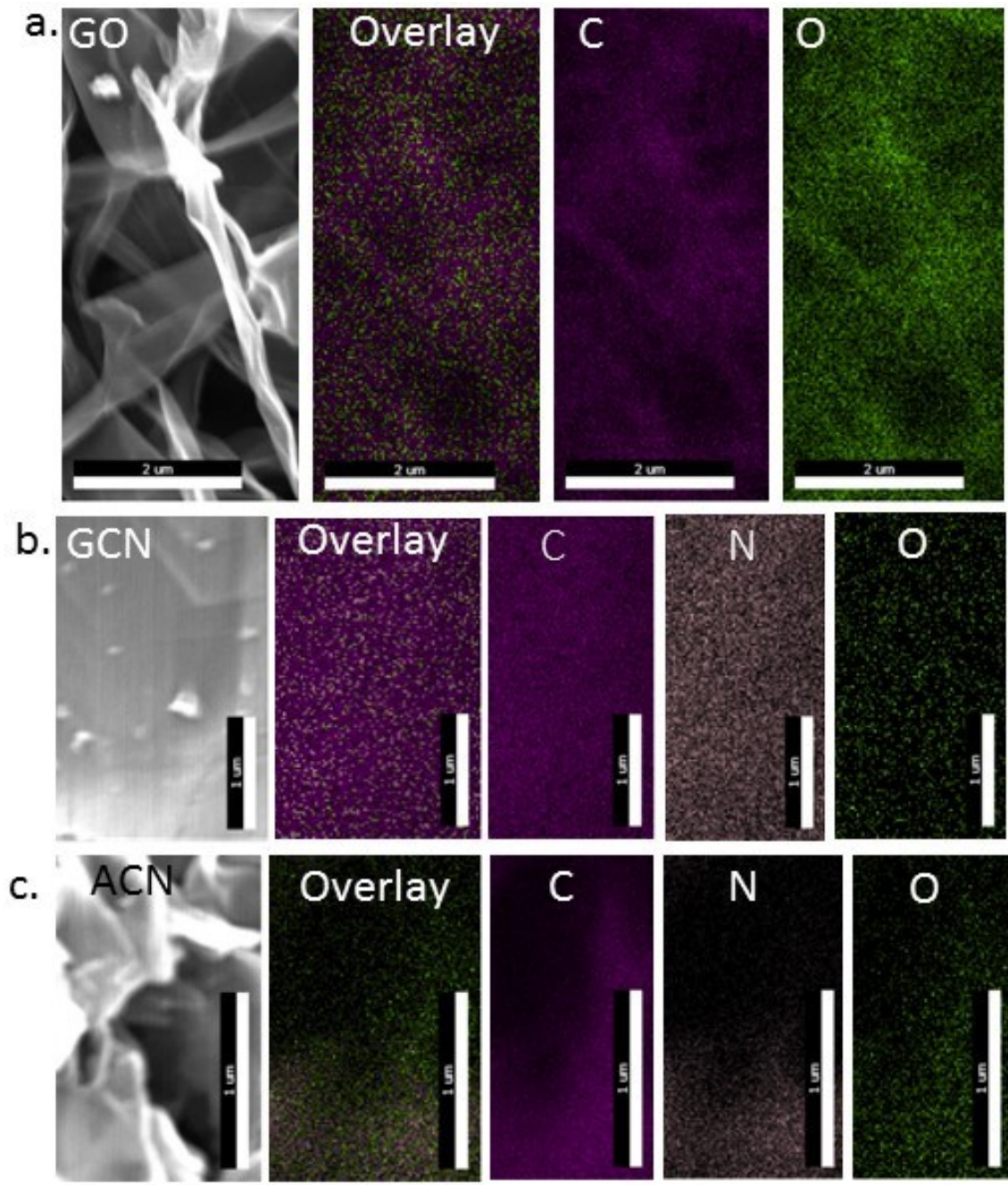
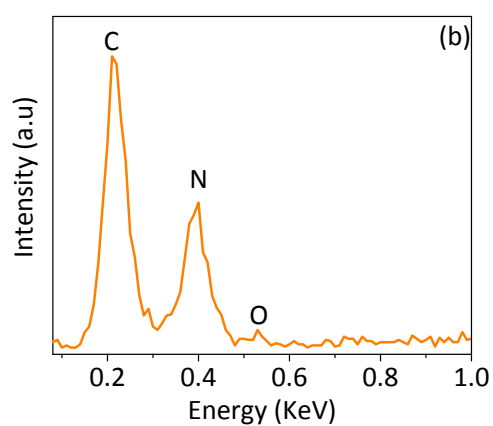
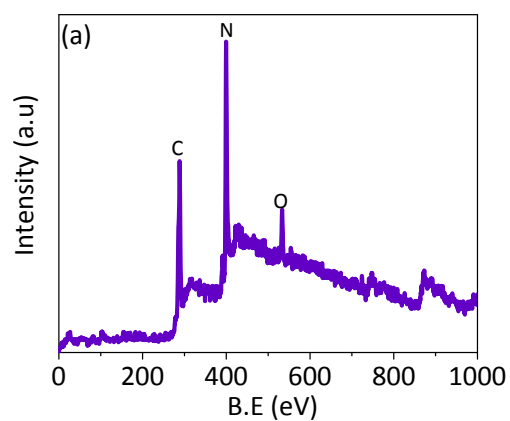
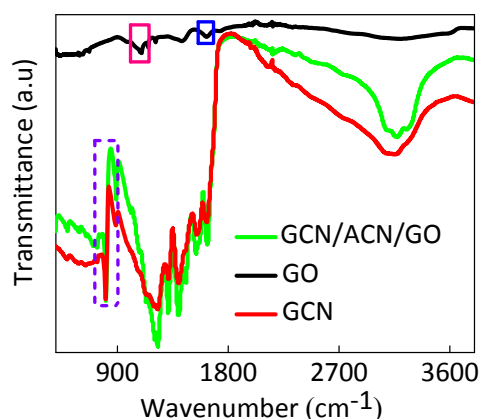


Fig. S4 EDX elemental mapping of (a) GO, (b) GCN and (c) ACN.



**Fig. S5 Elemental analysis of GCN/ACN/GO.** (a) XPS survey (b) EDS pattern of GCN/ACN/GO. The main elements are C and N with little adsorbed oxygen. The EDS elemental composition calculation is calibrated with 5 % error.



**Fig. S6** FTIR spectra of GO, GCN and GCN/ACN/GO.

The functional groups present in GO are aromatic C-H deformation bands at  $900\text{ cm}^{-1}$ , C-O stretching vibration at  $1076\text{ cm}^{-1}$ , phenolic C-OH stretching vibration at  $1210\text{ cm}^{-1}$ , tertiary alcoholic C-OH bending at  $1425\text{ cm}^{-1}$ , water H-O-H bending at  $1625\text{ cm}^{-1}$ , C=O stretching at  $1725\text{ cm}^{-1}$ , and O-H stretching vibration between  $3000\text{ to }3600\text{ cm}^{-1}$ .<sup>17, 18</sup> Due to presence of oxygen functional groups, GO exhibited brown colour when dissolved in water.<sup>17</sup> There are no C-O and C=O functional groups in either GCN or GCN/ACN/GO except breathing mode of triazine units between  $800 - 900\text{ cm}^{-1}$ , C-N heterocycles vibration and C=N bonds between  $1000\text{ to }1600\text{ cm}^{-1}$ , and uncondensed amino groups and surface absorbed water molecules between  $3000\text{ to }3600\text{ cm}^{-1}$ .<sup>19-23</sup> The absence of oxygen functional groups evidences the partial reduction of GO.<sup>3, 4, 17</sup>

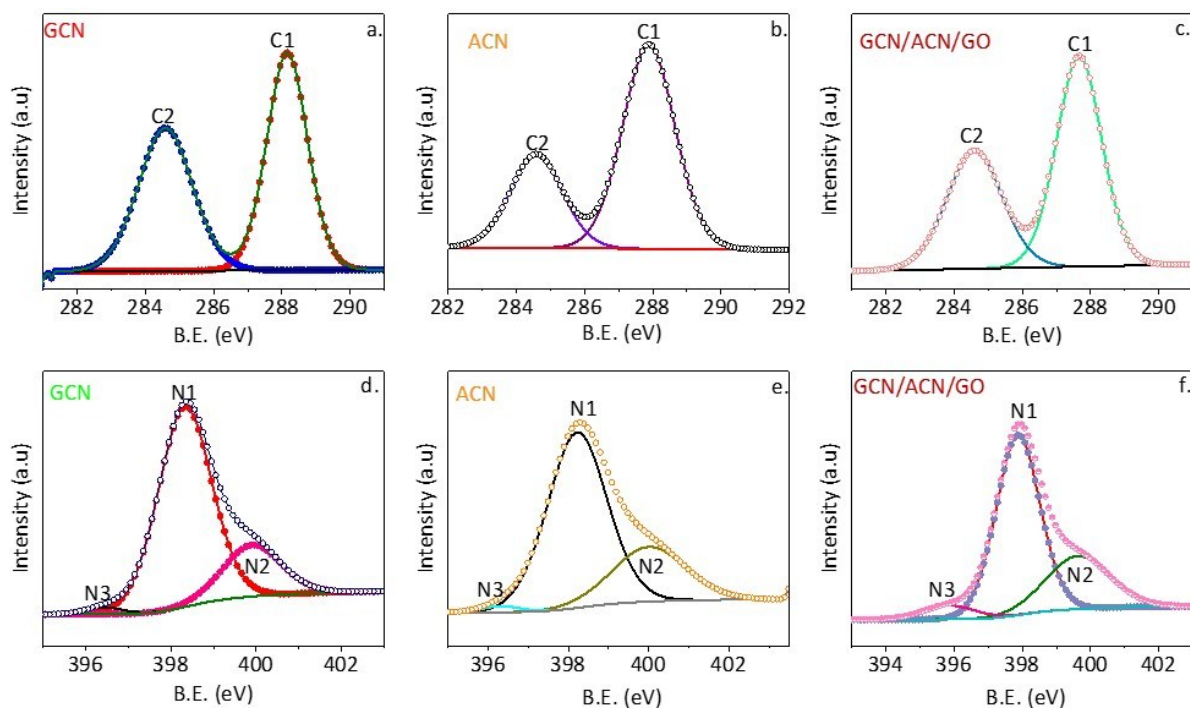


**Fig. S7** Top row is representing deconvoluted XPS C1s spectra for (a) GCN, (b) ACN and (c) GCN/ACN/GO. Bottom row is representing deconvoluted XPS N1s spectra for (d) GCN, (e) ACN and (f) GCN/ACN/GO.

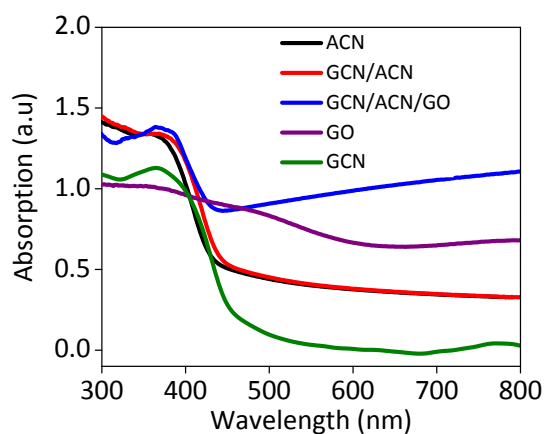


**Fig. S8** UV-vis diffuse reflectance spectra.

The significantly improved light absorption in the range of 500 – 800 nm in case of ACN is attributed with absence of long-range atomic arrangements. The absence of long-range atomic arrangement results a shift in conduction band and narrow the effective bandgap.<sup>24</sup>

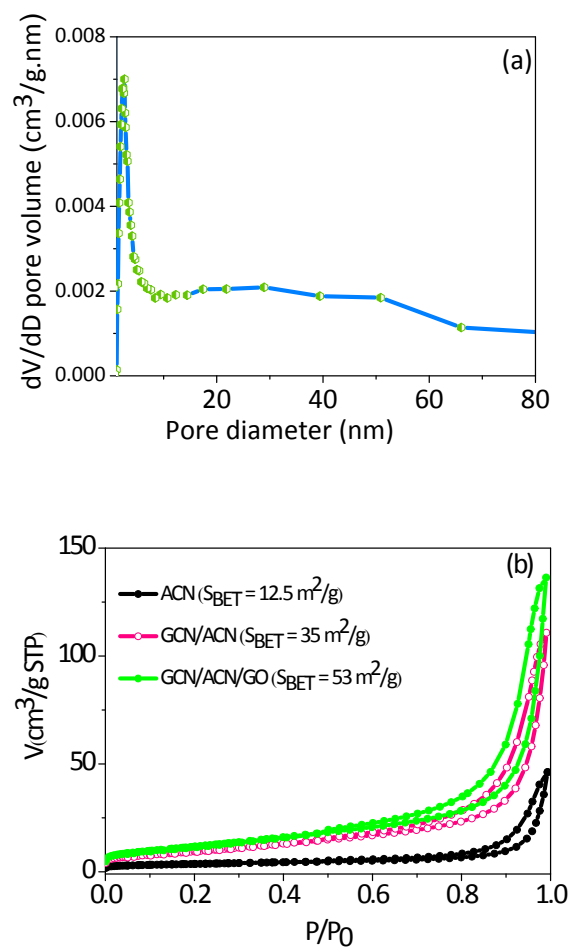


**Fig. S9 Pore size and surface area analysis.** (a) BJH pore size distribution of GCN/ACN/GO and (b)  $\text{N}_2$  adsorption-desorption isotherm of ACN, GCN/ACN and GCN/ACN/GO.

The binary GCN/ACN is nanosheet-like structure, therefore with the greater surface area than the bulk ACN. After incorporating GO into the GCN/ACN framework, the effective surface area increases further due to the large surface area of graphene.<sup>2, 25, 26</sup>

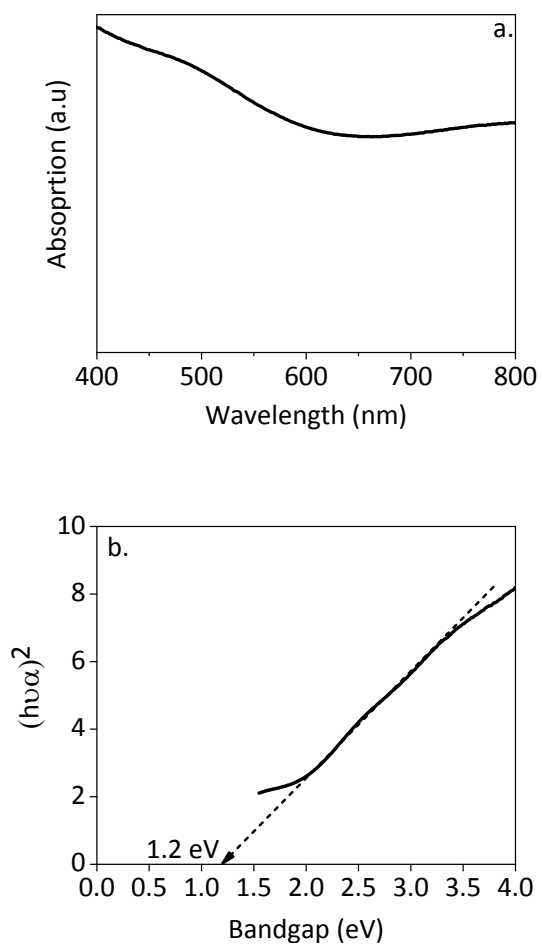


**Fig. S10** (a) UV-Vis spectra and (b) Kubelka-Munk plot of GO.

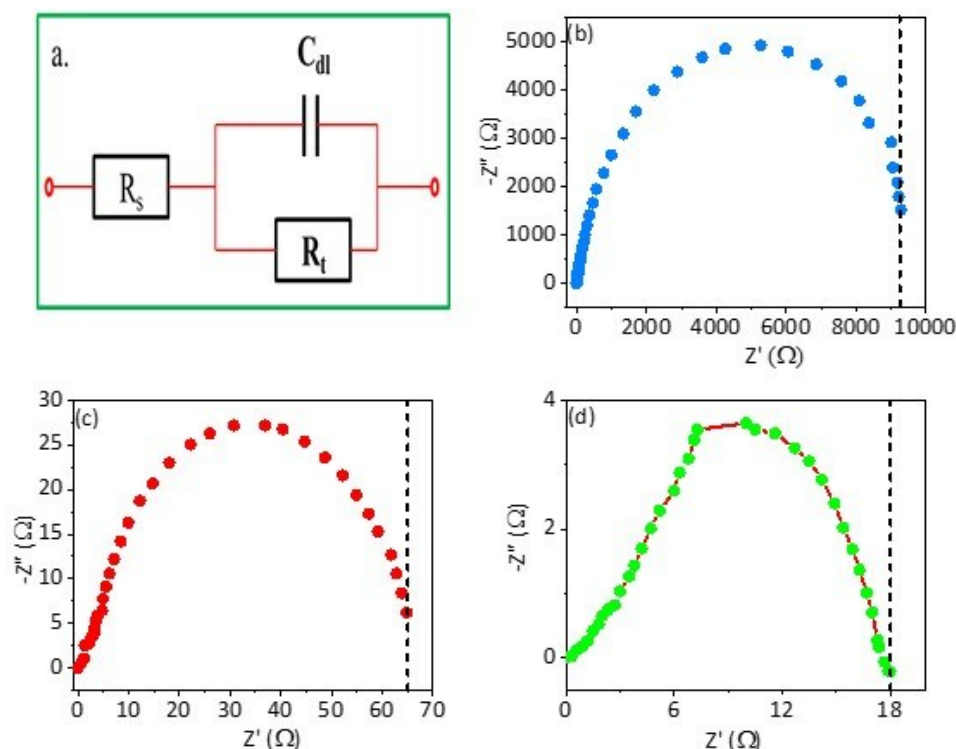


**Fig. S11 Nyquist plot obtained in a 0.5 M  $\text{Na}_2\text{SO}_4$  aqueous solution.** (a) Equivalent electric circuit model for simulation of semicircle in the Nyquist plot. Here, the  $R_s$  is the electrolyte solution resistance,  $R_t$  is the charge-transfer resistance of photocatalyst and  $C_{dl}$  is the double-layer capacitance. (b) Nyquist plot for ACN where the vertical black broken line is showing the approximated charge-transfer resistance,  $R_t$ . (c) Nyquist plot for GCN/ACN. The vertical black broken line shows the approximated charge-transfer resistance,  $R_t$  which is over 15 times lower than that of ACN, indicating GCN/ACN gains an improvement in charge-transfer efficiency. (d) Nyquist plot for GCN/ACN/GO. The vertical black broken line is shows the approximated charge-transfer resistance,  $R_t$  which is over 55 times lower than ACN and 3.6 times that for GCN/ACN. This lower charge-transfer resistance is an indication of improved charge-transfer efficiency, which is one of the driving forces behind enhancing the hydrogen production.

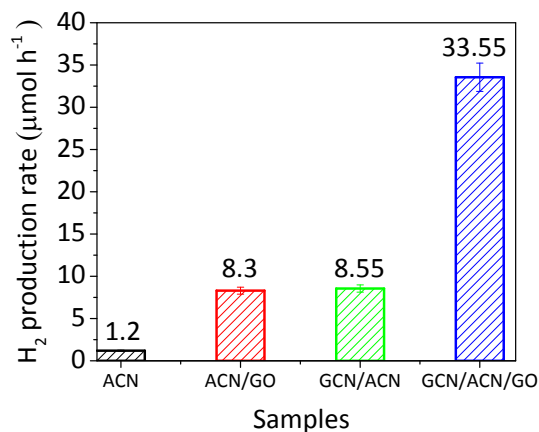


**Fig. S12 Comparison of Hydrogen production rate under visible light irradiation ( $\lambda = 420$  nm).** The reaction system consists of suspended 50 mg photocatalyst on 80 mL of 10 vol% triethanolamine. No cocatalyst has been used.

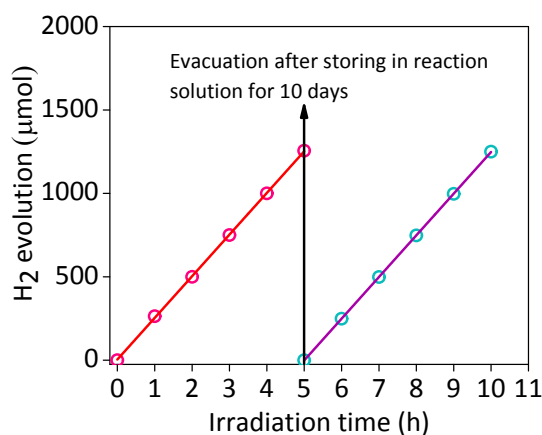


**Fig. S13 Hydrogen production stability estimation on GCN/ACN/GO under visible light irradiation ( $\lambda = 420$  nm).** The reaction system consists of suspended 50 mg photocatalyst on 80 mL of 10 vol% triethanolamine and *in-situ* photodeposited 3 wt% Pt as co-catalyst.

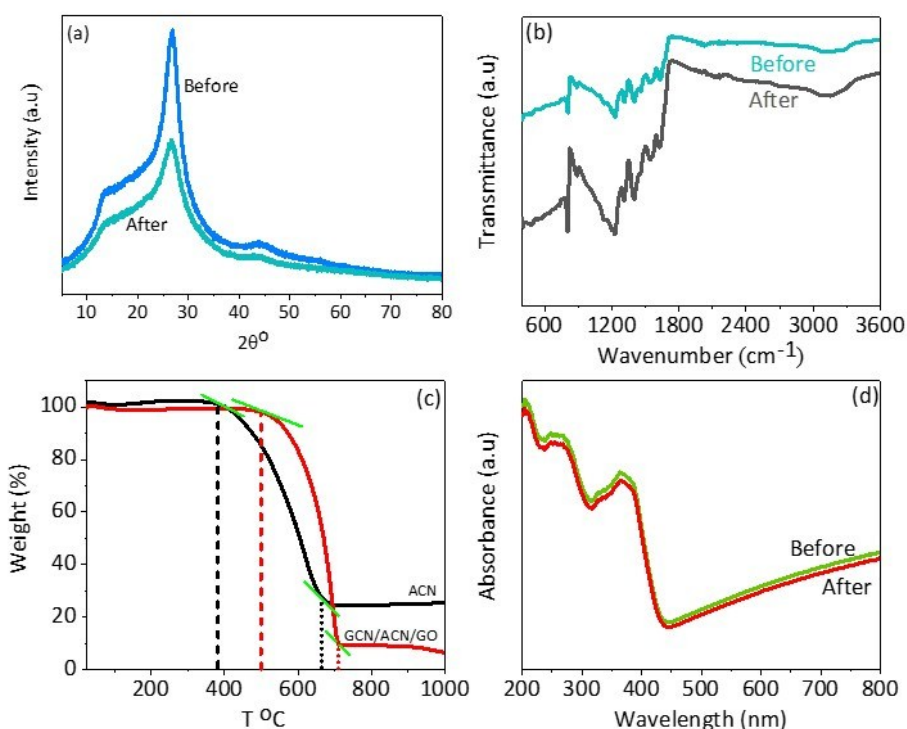


**Fig. S14 Structural, chemical and optical stability of GCN/ACN/GO.** (a) XRD pattern (b) FTIR spectra (c) TGA spectra (d) UV-vis spectra.

In addition to photocatalytic stability testing, the structural and thermal stability tests were performed also for GCN/ACN/GO heterostructure. As can be seen in the XRD and FTIR spectra taken before and after photocatalysis testing, there are no apparent changes in the structural motifs and bands of GCN/ACN/GO, except for reduced intensity. The thermogravimetric analysis confirmed that GCN/ACN/GO can withstand up to 700  $^\circ\text{C}$ . The TGA experiment was performed under  $\text{N}_2$  gas flow. For ACN, initial decomposition started at 390  $^\circ\text{C}$  - whereas it was 500  $^\circ\text{C}$  for GCN/ACN/GO. The GCN/ACN/GO underwent almost 100 % weight loss at 700  $^\circ\text{C}$  i.e. 40  $^\circ\text{C}$  greater than for parent ACN. This finding suggested that the hybridization with GCN and GO improved its stability.<sup>4</sup> The UV-Vis absorption spectra of used samples followed almost the same absorption edge for fresh samples; a reason for reproducible hydrogen without degradation during the three (3) runs for 15 h. These results confirm that as-prepared GCN/ACN/GO is a highly durable and stable photocatalyst for water splitting  $\text{H}_2$  production.

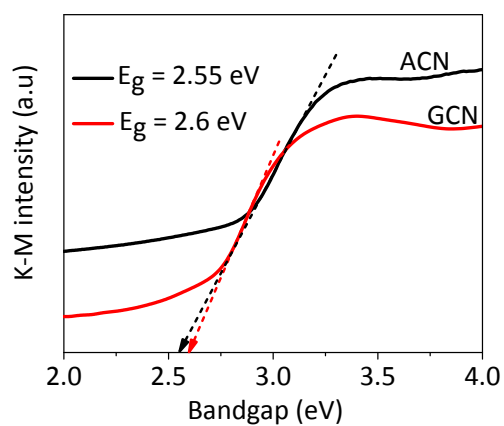


**Fig. S15** Kubelka-Munk (K-M) plot for bandgap calculation.

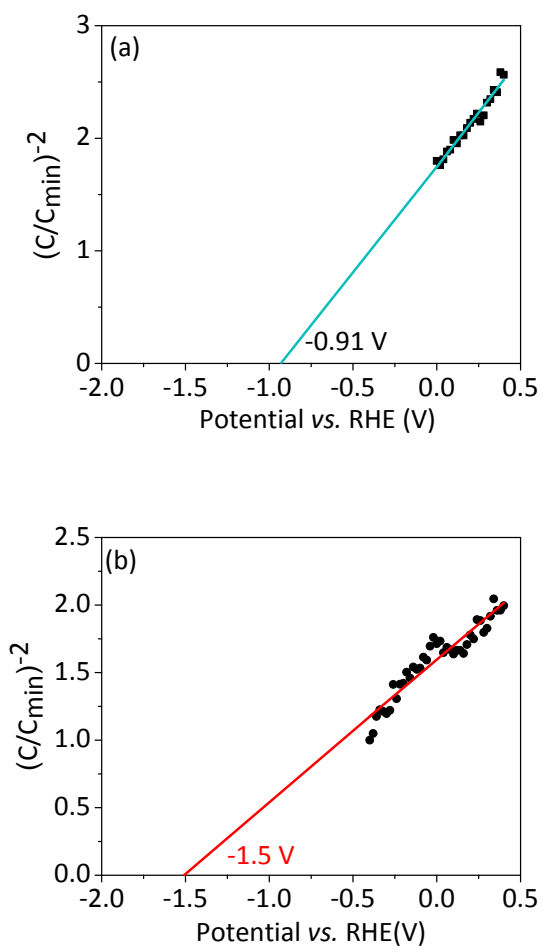


**Fig. S16** Extrapolated CB positions of (a) ACN and (b) GCN from Mott-Schottky plot.

## References

1. W. S. Hummers and R. E. Offeman, *J. Am. Chem. Soc.*, 1958, **80**, 1339-1339.
2. J. Duan, S. Chen, M. Jaroniec and S. Z. Qiao, *ACS Nano*, 2015, **9**, 931-940.
3. J. Zhang, L. Qi, J. Ran, J. Yu and S. Z. Qiao, *Adv. Energy Mater.*, 2014, **4**, 1301925.
4. Y. Hou, Z. Wen, S. Cui, X. Guo and J. Chen, *Adv. Mater.*, 2013, **25**, 6291-6297.
5. R. C. Pawar, V. Khare and C. S. Lee, *Dalton Trans.*, 2014, **43**, 12514-12527.
6. L. Wang, J. Ding, Y. Chai, Q. Liu, J. Ren, X. Liu and W.-L. Dai, *Dalton Trans.*, 2015, **44**, 11223-11234.
7. Y. Cui, H. Li, H. Miao, *Patent Nr. CN103736514A*, 2014.
8. T. Zhou, Y. Xu, H. Xu, H. Wang, Z. Da, S. Huang, H. Ji and H. Li, *Ceram. Int.*, 2014, **40**, 9293-9301.
9. Q. Gu, J. Long, H. Zhuang, C. Zhang, Y. Zhou and X. Wang, *Phys. Chem. Chem. Phys.*, 2014, **16**, 12521-12534.
10. H. Park, W. Choi and M. R. Hoffmann, *J. Mater. Chem.*, 2008, **18**, 2379-2385.
11. S. R. Lingampalli, U. K. Gautam and C. N. R. Rao, *Energy Environ. Sci.*, 2013, **6**, 3589-3594.
12. Z. Yan, X. Yu, A. Han, P. Xu and P. Du, *J. Phys. Chem. C*, 2014, **118**, 22896-22903.
13. X. Yao and X. Liu, *J. Hazardous Mater.*, 2014, **280**, 260-268.
14. W. Wang, J. C. Yu, D. Xia, P. K. Wong and Y. Li, *Environ. Sci. Technol.*, 2013, **47**, 8724-8732.
15. Y. Hou, J. Li, Z. Wen, S. Cui, C. Yuan and J. Chen, *Nano Energy*, 2014, **8**, 157-164.
16. S. W. Hu, Y. Tian, X. L. Wei, J. W. Ding, J. X. Zhong, L. W. Yang and P. K. Chu, *J. Colloid. Interface Sci.*, 2014, **431**, 42-49.
17. T.-F. Yeh, J.-M. Syu, C. Cheng, T.-H. Chang and H. Teng, *Adv. Funct. Mater.*, 2010, **20**, 2255-2262.
18. T.-F. Yeh, C.-Y. Teng, S.-J. Chen and H. Teng, *Adv. Mater.*, 2014, **26**, 3297-3303.
19. G. Algara-Siller, N. Severin, S. Y. Chong, T. Björkman, R. G. Palgrave, A. Laybourn, M. Antonietti, Y. Z. Khimiyak, A. V. Krasheninnikov, J. P. Rabe, U. Kaiser, A. I. Cooper, A. Thomas and M. J. Bojdys, *Angew. Chem. Int. Ed.*, 2014, **53**, 7450-7455.
20. A. Thomas, A. Fischer, F. Goettmann, M. Antonietti, J.-O. Muller, R. Schlogl and J. M. Carlsson, *J. Mater. Chem.*, 2008, **18**, 4893-4908.

21. D. Zheng, X. N. Cao and X. Wang, *Angew. Chem. Int. Ed.*, 2016, **55**, 11512-11516.
22. M. Shalom, S. Inal, C. Fettkenhauer, D. Neher and M. Antonietti, *J. Am. Chem. Soc.*, 2013, **135**, 7118-7121.
23. M. Z. Rahman, J. Ran, Y. Tang, M. Jaroniec and S. Z. Qiao, *J. Mater. Chem. A*, 2016, **4**, 2445-2452.
24. Y. Kang, Y. Yang, L.-C. Yin, X. Kang, G. Liu and H.-M. Cheng, *Adv. Mater.*, 2015, **27**, 4572-4577.
25. Q. Xiang, J. Yu and M. Jaroniec, *J. Phys. Chem. C*, 2011, **115**, 7355-7363.
26. X. Wang, G. Zhang and Z. A. Lan, *Angew. Chem. Int. Ed.*, 2016, DOI: 10.1002/anie.201607375.